Electronic Supplementary Information

Experimental

Materials: Condensed acetic acid (CH_3COOH), NaOH, HCl, Na_2SO_4, and C_2H_5OH were purchased from Chengdu Kelong Chemical Reagent Factory. Manganese (II) acetate ($Mn(CH_3COO)_2$), potassium chlorate ($KClO_3$), sodium salicylate ($C_7O_3H_5Na$), sodium hypochlorite (NaClO), sodium nitroferricyanide dihydrate ($C_5FeN_6Na_2O{\cdot}2H_2O$), para-(dimethylamino) benzaldehyde (p-$C_9H_{11}NO$), and $N_2H_4{\cdot}H_2O$ were purchased from Aladdin Ltd. (Shanghai, China). TM purchased from Hongshan District, Wuhan Instrument Surgical Instruments business. The water used throughout all experiments was purified through a Millipore system. All chemicals were used as received without further purification.

Preparation of MnO_2 NA/TM and MnO_x NA/TM: MnO_2 NA/TM was prepared as follows. 5 mL CH_3COOH was diluted into 70 mL aqueous solution. Then, 5 mmol $Mn(CH_3COO)_2$ and 8.75 mmol $KClO_3$ were added to the above solution. Then the solution was transferred into a Teflon-lined stainless autoclave (100 mL), and a piece of TM was immersed into the autoclave contained solution. The autoclave was sealed and maintained at 160 °C for 12 h in an electric oven. After the autoclave cooled down naturally to room temperature, the resulting MnO_2 NA/TM was taken out and washed with deionized water and C_2H_5OH several times alternatively, then dried in air at 60 °C for 6 h. To obtain MnO_x NA/TM, MnO_2 NA/TM was then calcinated at 350 °C for 2 h with heating rate of 2 $^oC\ min^{-1}$ in Ar flow. The average loading for MnO_x on TM was determined to be 1.1 mg cm^{-2}.

Characterizations: XRD patterns were obtained from a Shimazu XRD-6100 diffractometer with Cu Kα radiation (40 kV, 30 mA) of wavelength 0.154 nm (Japan). SEM images were collected from the tungsten lamp-equipped SU3500 scanning electron microscope at an accelerating voltage of 20 kV (HITACHI, Japan). TEM images were obtained from a Zeiss Libra 200FE transmission electron microscope operated at 200 kV. XPS measurements were performed on an ESCALABMK II X-ray photoelectron spectrometer using Mg as the exciting source. The UV-Vis

absorbance spectra were measured on a SHIMADZU UV-1800 UV-Vis spectrophotometer. Raman spectra were collected on Renishaw with a 514.5 nm laser. A gas chromatograph (SHIMADZU, GC-2014C) equipped with MolSieve 5A column and Ar carrier gas was used for H_2 quantification. The temperature programmed deoxidation (O_2-TPD) spectra were tested by TP-5076 TPD experimental device. Thermogravimetric (TG) curve were collected on a Perkin-Elmer Model Pyris1 TG analyzer at a heating rate of 10 °C min^{-1} in flowing Ar. ^1H nuclear magnetic resonance (^1H NMR) spectra were collected on a superconducting-magnet NMR spectrometer (Bruker AVANCE III HD 500 MHz) and dimethyl sulphoxide was used as an internal to calibrate the chemical shifts in the spectra.

Electrochemical Measurements: Before NRR tests, the Nafion proton exchange membrane was pretreated by heating in 3% H_2O_2 solution, 0.5 M H_2SO_4 and ultrapure water at 80 °C for 1 h, respectively. Electrochemical measurements were performed on a CHI 660E electrochemical analyzer (CHI Instruments, Inc., Shanghai) in a standard three-electrode system using MnO_2 NA/TM, MnO_x NA/TM or TM as working electrode, Ag/AgCl as reference electrode, and graphite rod as counter electrode. All experiments were carried out at ambient conditions. For N_2 reduction experiments, the Na_2SO_4 electrolyte (0.1 M) was bubbled with high-purity N_2 for 30 min before measurement. All potentials reported in this work were calibrated to RHE, using the following equation:

$$E\ (RHE) = E\ (Ag/AgCl) + (0.197 + 0.059\ pH)\ V$$

Determination of NH_3: NH_3 concentration was determined by the indophenol blue method.[1] In detail, 4 mL of post-NRR solution was removed from the cathodic chamber. Then, 50 μL oxidizing solution (NaClO (ρ_{Cl}=4~4.9) and 0.75 M NaOH), 500 μL coloring solution (0.4 M $C_7H_5O_3Na$ and 0.32 M NaOH), and 50 μL catalyst solution (0.1 g $Na_2[Fe(CN)_5NO]\cdot 2H_2O$ diluted to 10 mL with deionized water) were added to the sample solution, sequentially. After standing the mixture solution at 25 °C for 1 h, UV-Vis absorption spectra were measured at a wavelength of 660 nm. The concentration-absorbance curve was calibrated using standard ammonia solutions with a series of concentrations. The fitting curve ($y = 0.716x + 0.017$, $R^2 = 0.999$)

shows good linear relation of absorbance value with NH_3 concentration by three times independent calibrations.

Determination of N_2H_4: Concentration of N_2H_4 in the electrolyte was estimated by the method of Watt and Chrisp.[2] In brief, a mixture solution containing p-$C_9H_{11}NO$ (5.99 g), concentrated HCl (30 mL) and ethanol (300 mL) was used as a color reagent. In detail, 5 mL electrolyte removed from the cathodic chamber was added into 5 mL above prepared color reagent. After standing the mixture solution at 25 °C for 10 min, UV-Vis absorption spectra were measured at a wavelength of 455 nm. The concentration-absorbance curves were calibrated using standard N_2H_4 solutions with a series of concentrations for three independent calibrations.

Calculations of NH_3 yield rate and FE: NH_3 yield was calculated using the following equations:

$$R_{NH3}\ (\text{mol cm}^{-2}\ \text{s}^{-1}) = (c_{NH3} \times V) / (17 \times t \times A)$$

or

$$R_{NH3}\ (\mu\text{g h}^{-1}\ \text{mg}^{-1}_{\text{cat.}}) = (c_{NH3} \times V) / (17 \times t \times m)$$

Where c_{NH3} (μg mL^{-1}) is the measured NH_3 concentration; V (mL) is the volume of electrolyte; t (s or h) is the reaction time; A (cm^2) is the geometric area of the cathode; m (mg) is the mass loading of catalyst on TM.

FE was calculated according to following equation:

$$FE = 3 \times F \times c_{NH3} \times V / (17 \times Q) \times 100\%$$

Calculation of ECSA: Electrochemical capacitance measurement was used to acquire the active surface area of MnO_x NA/TM and MnO_2 NA/TM. The specific capacitance can be converted into an ECSA using the following equation:

$$A_{ECSA} = C_{dl} / 60\ \mu\text{F cm}^{-2}\ \text{per cm}^2_{ECSA}$$

V_O Determination: First, the Mn^{x+}/Mn^{4+} ratio was calculated from peak areas. In general, the existence of low-valent Mn in MnO_x indicates the oxygen vacancies will be generated to maintain electrostatic balance according to the following chemical equation:

$$6Mn^{4+} + 2O^{2-} \rightarrow 6Mn^{4+} + 4e^-/2\square + O_2 \rightarrow 3Mn^{4+} + 2Mn^{3+} + Mn^{2+} + 2\square + O_2$$

The □ represents an empty position originating from the removal of O^{2-} in the lattice.

It can be deduced that two oxygen vacancies generated companied with one Mn^{2+} and two Mn^{3+} ions from the equation.

Computational details: All DFT calculations were performed using the Vienna ab initio simulation package (VASP).[3-5] The exchange correlation is described by the Perdew, Burke, and Ernzerhof functional within the generalized gradient approximation (PBE-GGA).[6] The projector-augmented wave (PAW)[7,8] method is used to represent the core-valence electron interaction. The calculations are also conducted involving long-range dispersion interactions (DFT-D3 (BJ)). A Hubbard U term is added to the PBE functional (DFT+U), and a value of U_{eff} = 4.5 eV is employed for Mn on its d orbital according to previous literatures.[9,10] Manganese 3d, 4s, nitrogen 2s, 2p, and oxygen 2s, 2p electrons are treated as valence electrons and an energy cutoff of 400 eV for basis-set expansion is used. The MnO_2 (310) surface is modeled as a periodic slab with three trilayers, and the vacuum between slabs is 15 Å. A 4×1 surface cell and the corresponding 1 × 1 × 1 k-point mesh are used in the calculations. The adsorption processes are modelled on one side of the slabs and during structural optimization, all of the atoms, except those in the bottom MnO_2 trilayer of the slabs, are allowed to relax until atomic forces reached below 0.05 eV $Å^{-1}$. Adsorption energies are calculated by the following equation: $E_{ads} = - (E_{total} - E_{surface} - E_{gas})$ where E_{total}, $E_{surface}$ and E_{gas} are the calculated electronic energies of the adsorbed species on the surface, a clean surface and a gas phase molecule, respectively. The ΔG value are calculated as follows:

$$\Delta G = \Delta E + \Delta ZPE - T\Delta S$$

where ΔE is the difference of electronic energy, ΔZPE is the change in zero-point energies, T is the temperature (T = 298.15K), and ΔS is the change of entropy. The zero-point energies and entropies of the NRR species are calculated from the vibrational frequencies of adsorbed species. The entropies and vibrational frequencies of molecules in the gas phase are from the NIST database. [http://cccbdb.nist.gov/]

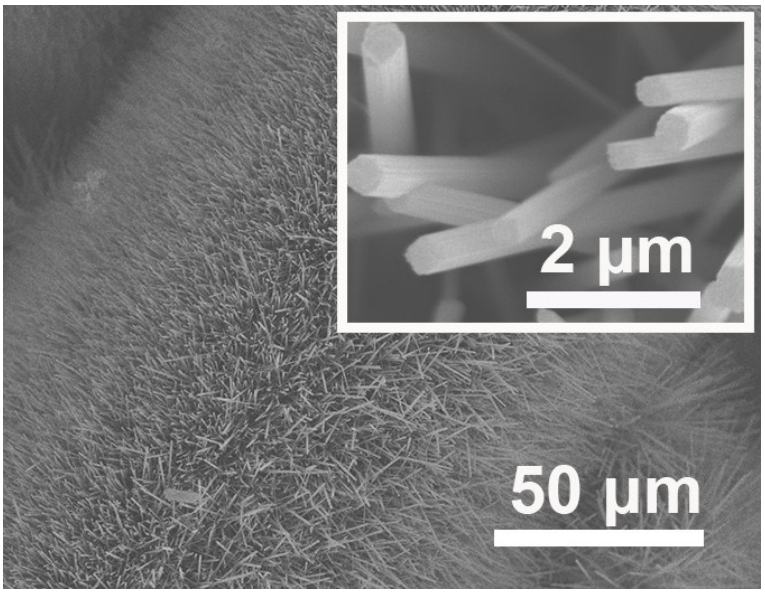

Fig. S1. SEM images of pristine MnO_2 NA/TM.

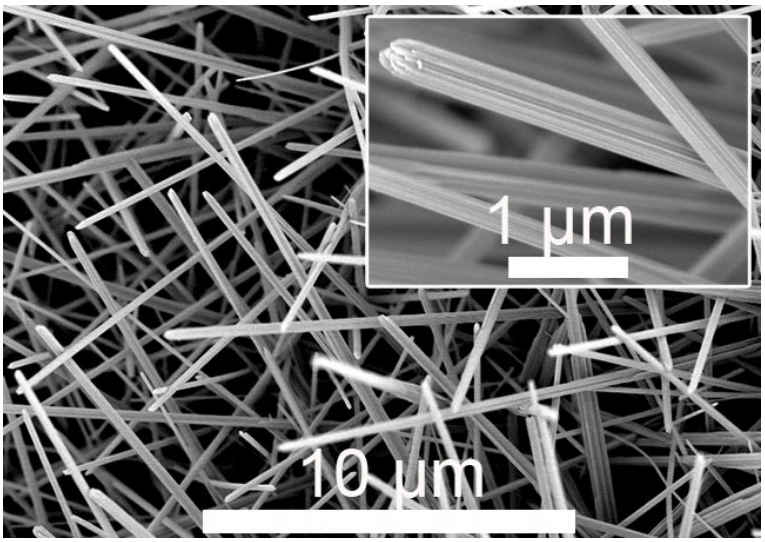

Fig. S2. Field-emission SEM images of pristine MnO_x NA/TM.

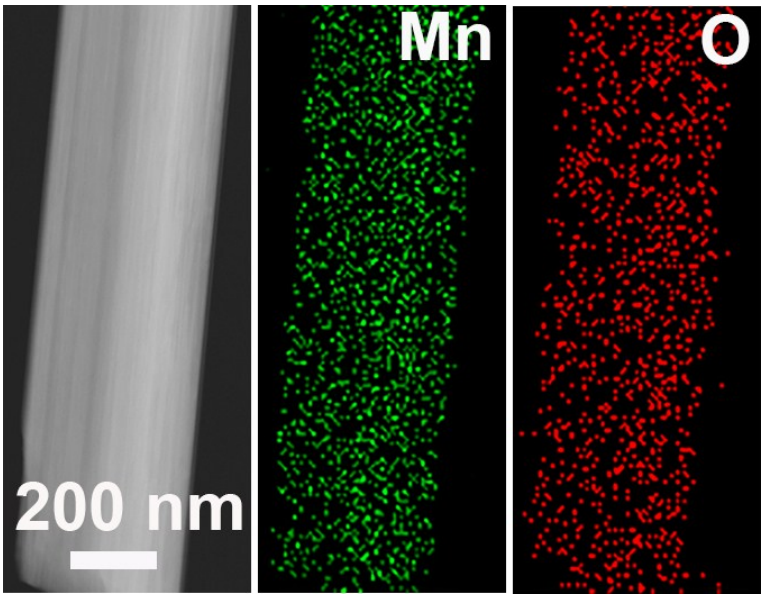

Fig. S3. STEM and corresponding energy-dispersive X-ray elemental mapping images for one single MnO_x nanowire.

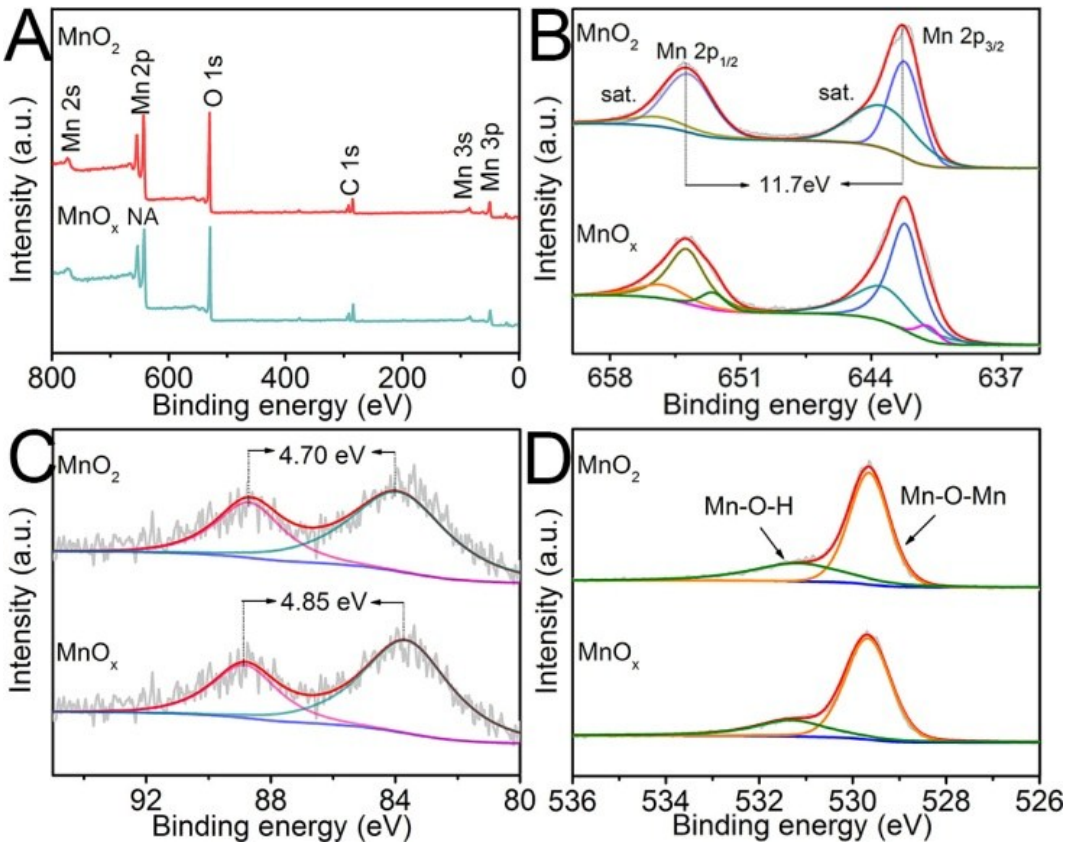

Fig. S4. (A) XPS survey spectra of MnO_2 and MnO_x. XPS spectra in (B) Mn 2p, (C) Mn 3s, and (D) O 1s regions.

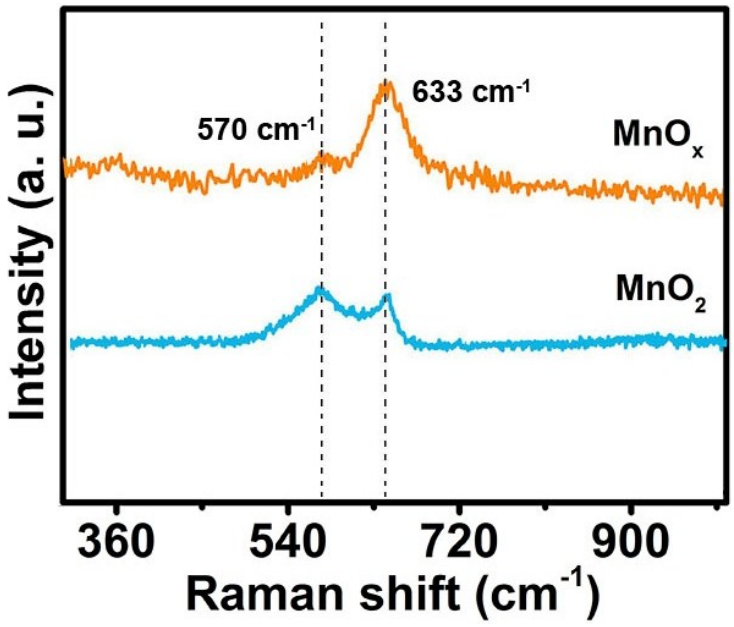

Fig. S5. Raman shift spectra of MnO_2 and MnO_x.

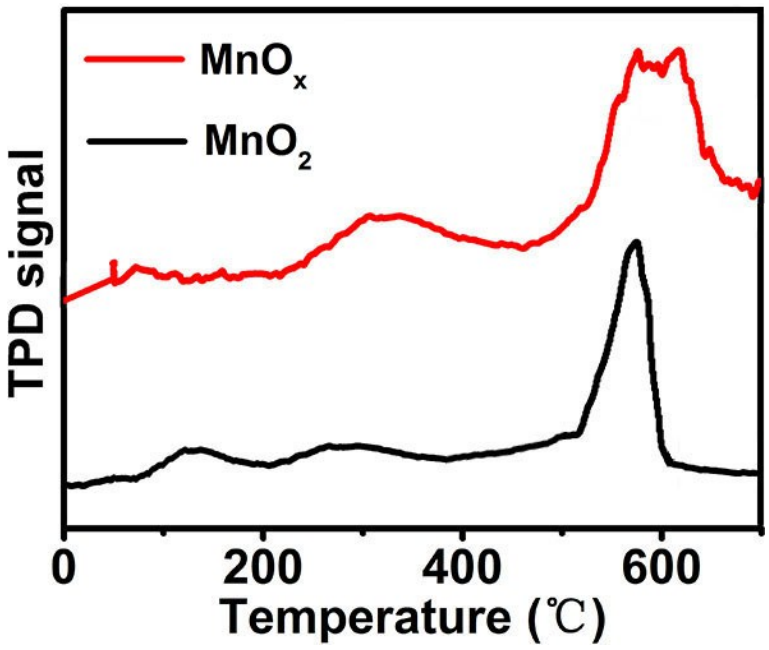

Fig. S6. O_2-TPD profiles of MnO_2 and MnO_x.

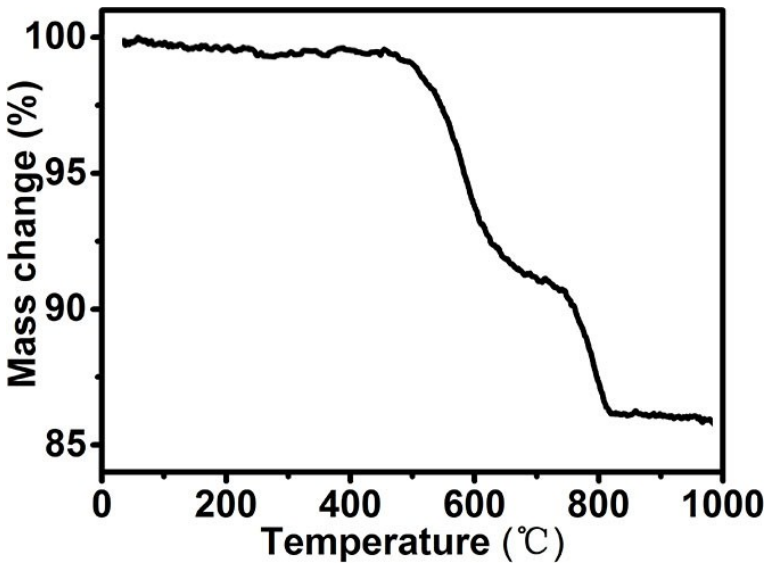

Fig. S7. TG curve of MnO_x.

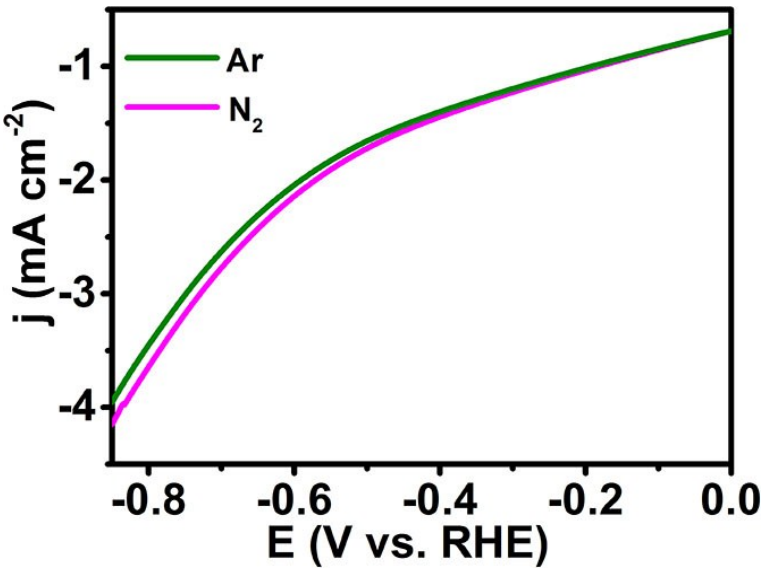

Fig. S8. Linear scan voltammetry curves of MnO_x NA/TM in Ar- and N_2-saturated 0.1 M Na_2SO_4.

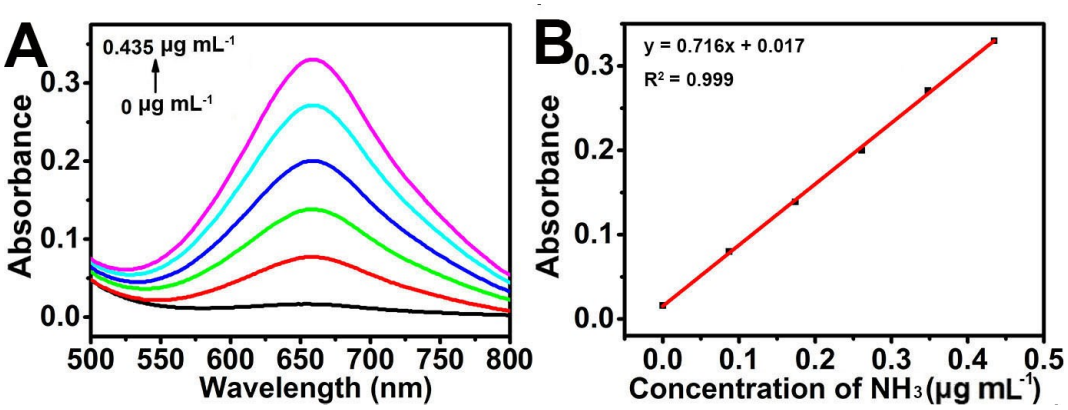

Fig. S9. (A) UV-Vis absorption spectra of indophenol assays with NH_3 in 0.1 M Na_2SO_4 after incubated for 1 hour at room temperature and (B) calibration curve used for estimation of NH_3.

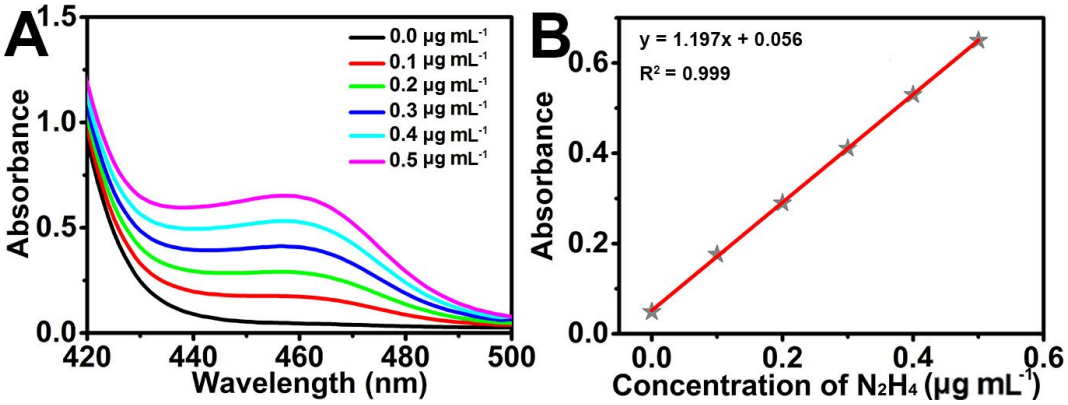

Fig. S10. (A) UV-Vis absorption spectra of various N_2H_4 concentration after incubated for 10 min at room temperature. (B) Calibration curve used for estimation of N_2H_4 concentration.

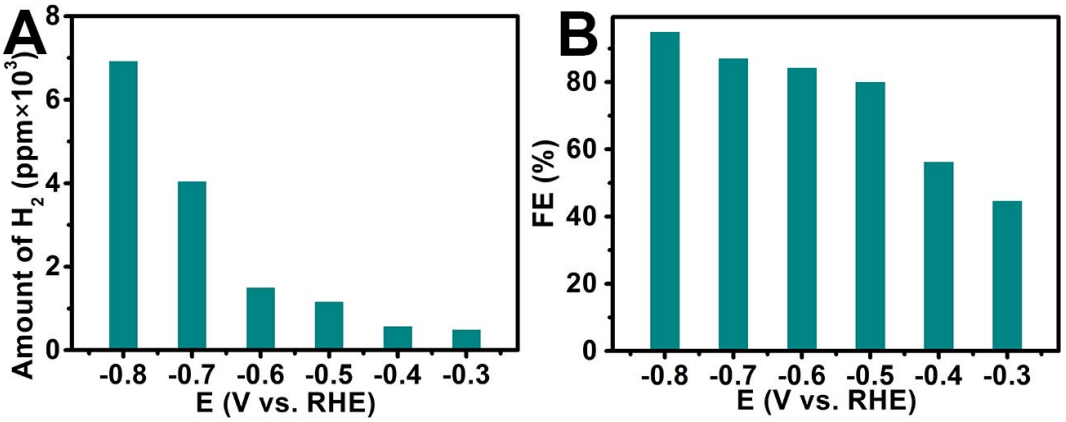

Fig. S11. (A) The amount of produced H_2 at each given potential. (B) The corresponding FE of H_2 at each given potential.

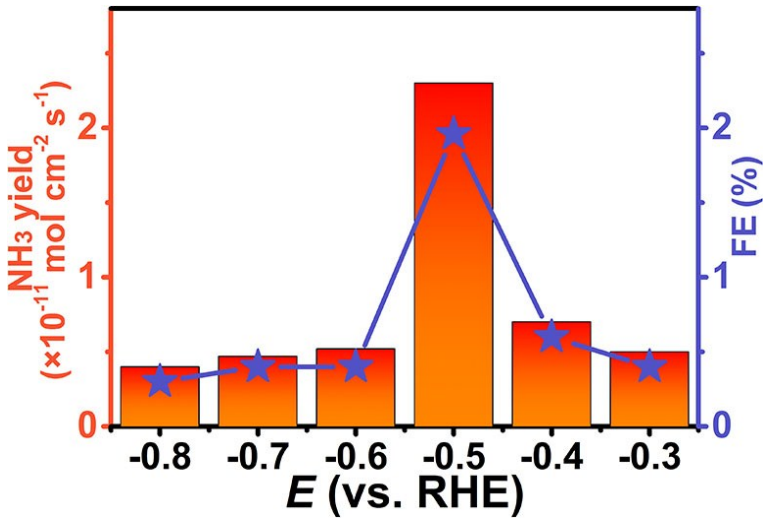

Fig. S12. NH_3 yields and FEs for pristine MnO_2 NA/TM at a series of potentials for 2 h electrolysis under ambient conditions.

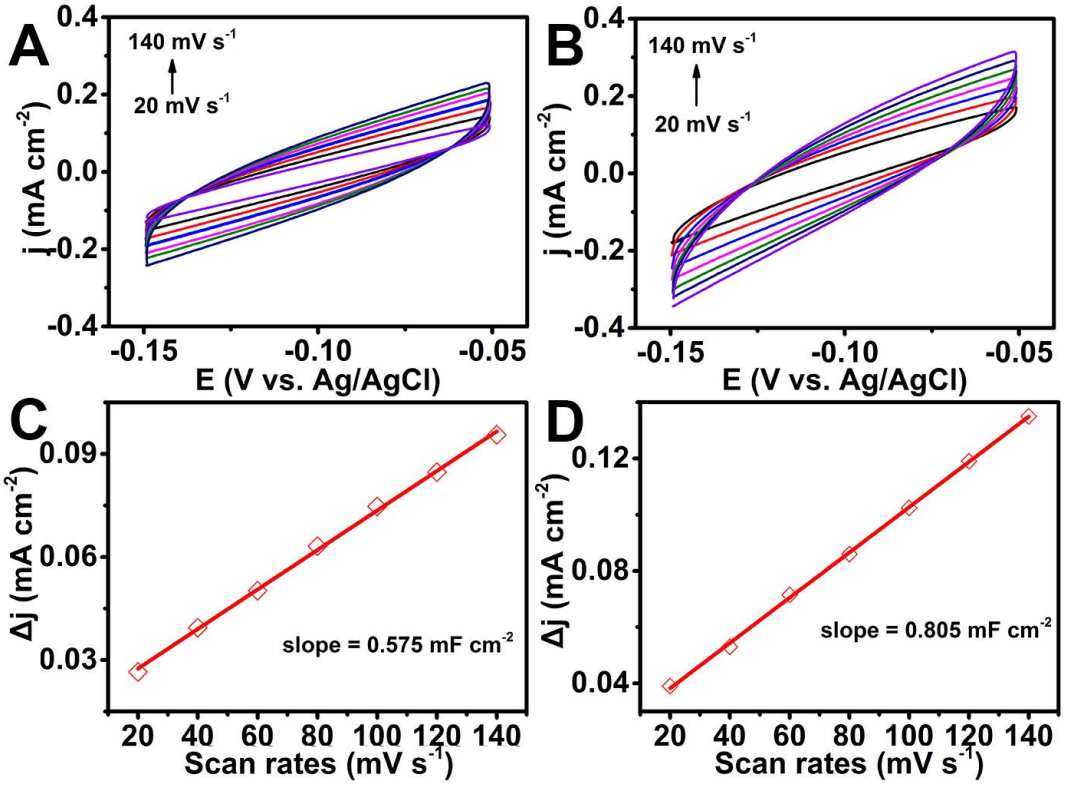

Fig. S13. Cyclic voltammograms for (A) MnO_2 NA/TM and (B) MnO_x NA/TM in the non-faradaic capacitance current range at scan rates of 20, 40, 60, 80, 100, 120, and 140 mV s^{-1}. The capacitive currents at –0.10 V vs. Ag/AgCl as a function of scan rate for (C) MnO_2 NA/TM and (D) MnO_x NA/TM.

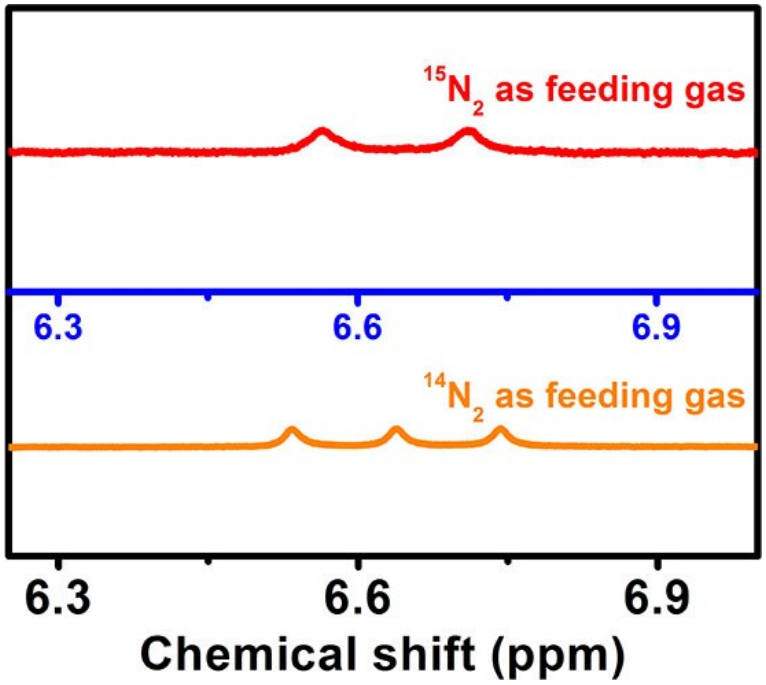

Fig. S14. ^{15}N isotope labeling experiment. ^{1}H NMR spectra for the post-electrolysis 0.1 M Na_2SO_4 electrolytes with $^{15}N_2$ and $^{14}N_2$ as feeding gas.

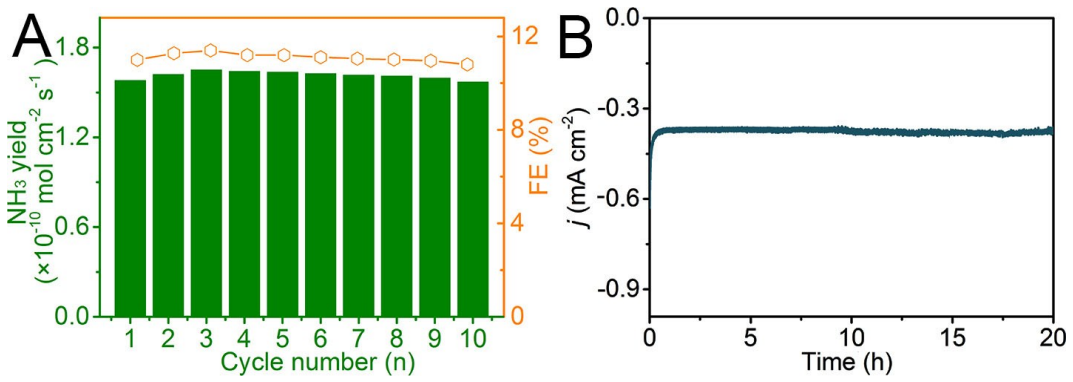

Fig. S15. (A) Cycling test of MnO_x NA/TM at −0.5 V vs. RHE. (B) *i-t* curve of MnO_x NA/TM for NRR at −0.5 V vs. RHE for 20 h.

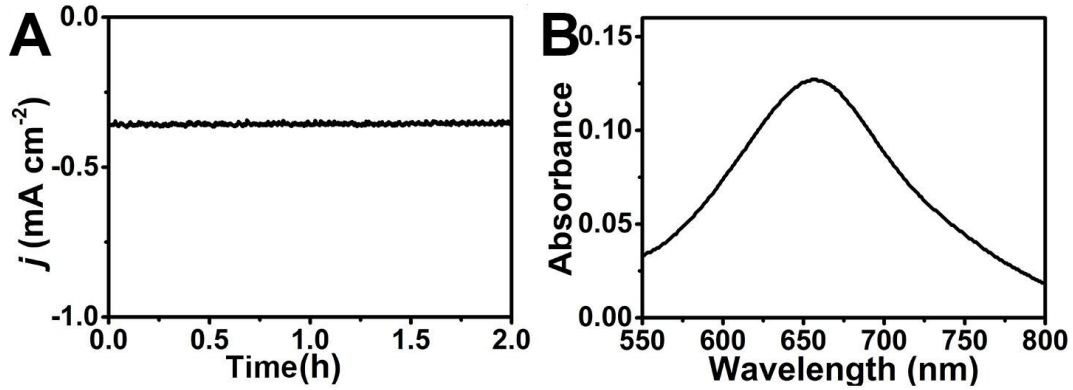

Fig. S16. (A) Chronoamperometric curve of MnO_x NA/TM after long-term electrolysis at −0.5 V. (B) UV-Vis absorption spectrum of corresponding electrolyte.

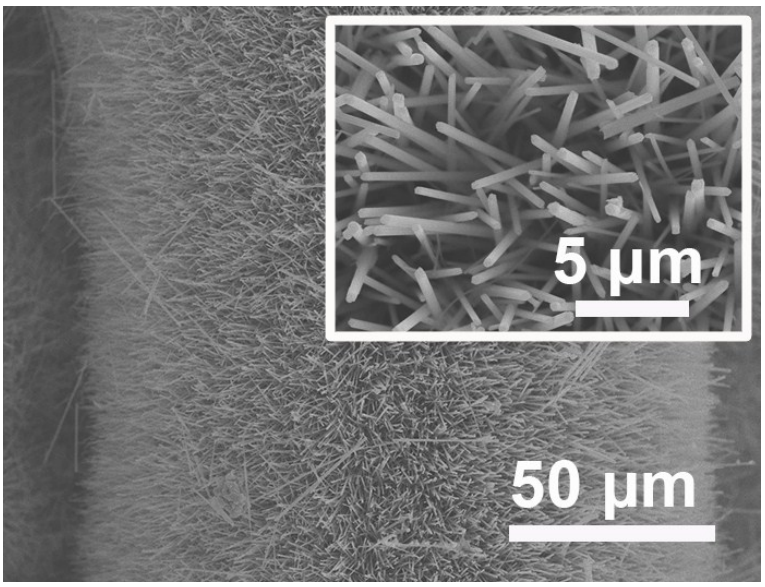

Fig. S17. SEM images of MnO_x NA/TM after stability test.

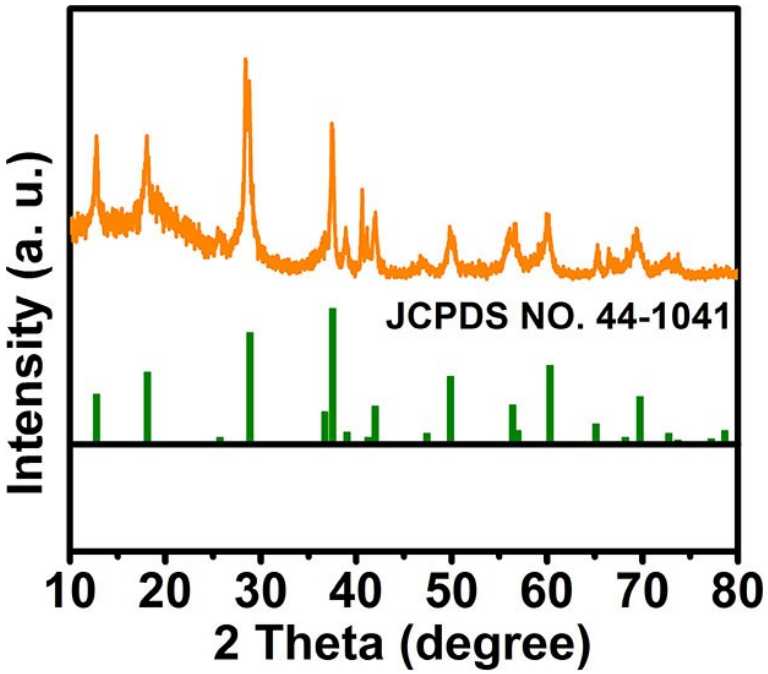

Fig. S18. XRD pattern of MnO_x after stability test.

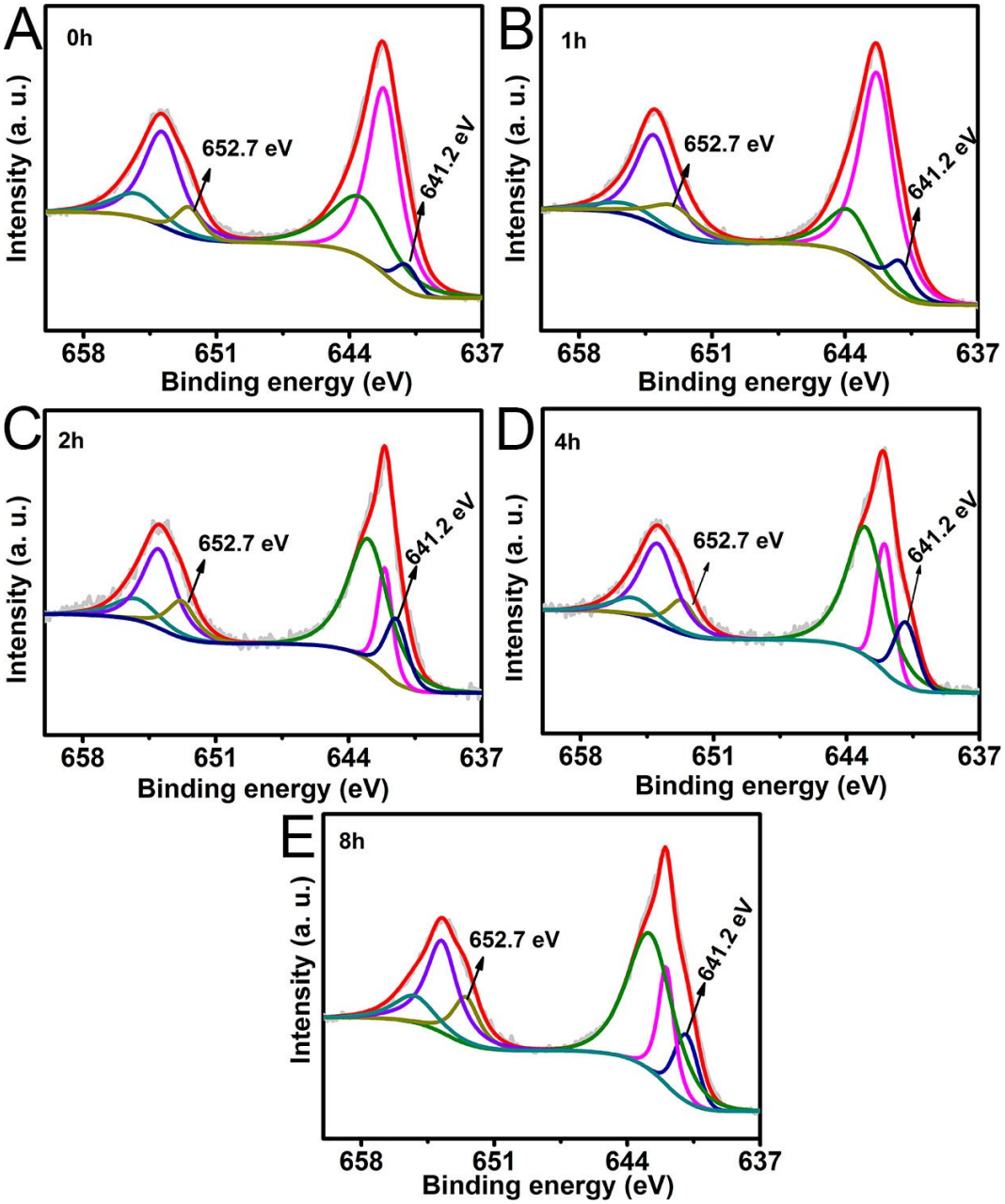

Fig. S19. XPS spectra of MnO_x in Mn 2p region before and after electrolysis at –0.5 V for different time.

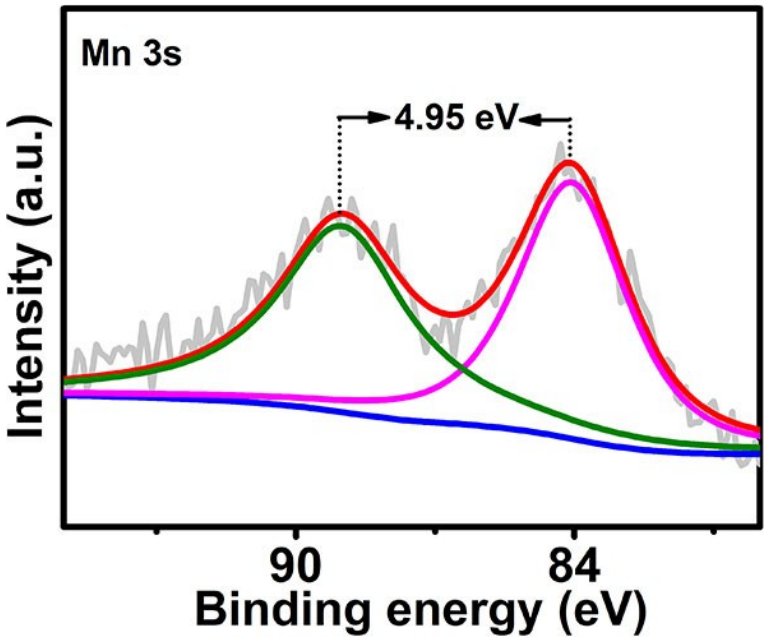

Fig. S20. XPS spectrum of MnO_x in Mn 3s region after stability test at –0.5 V.

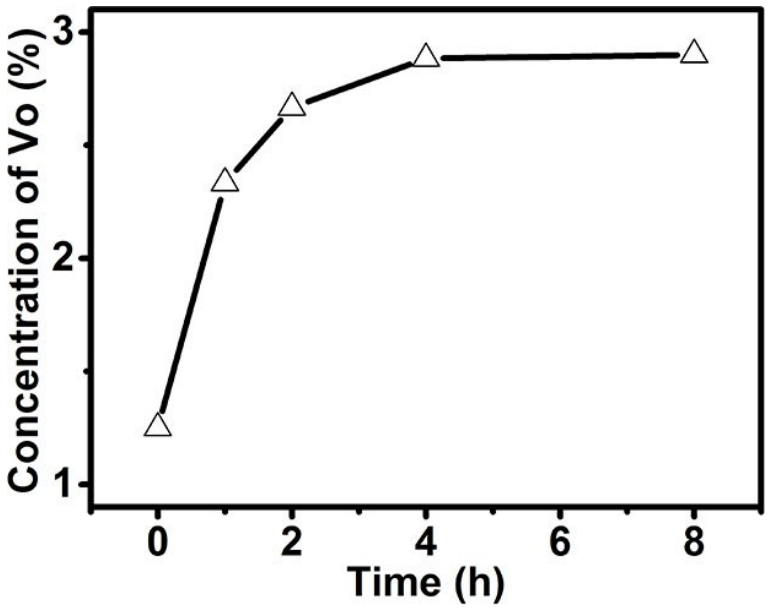

Fig. S21. Concentrations of V_O in MnO_x after electrolysis for different time at – 0.5 V.

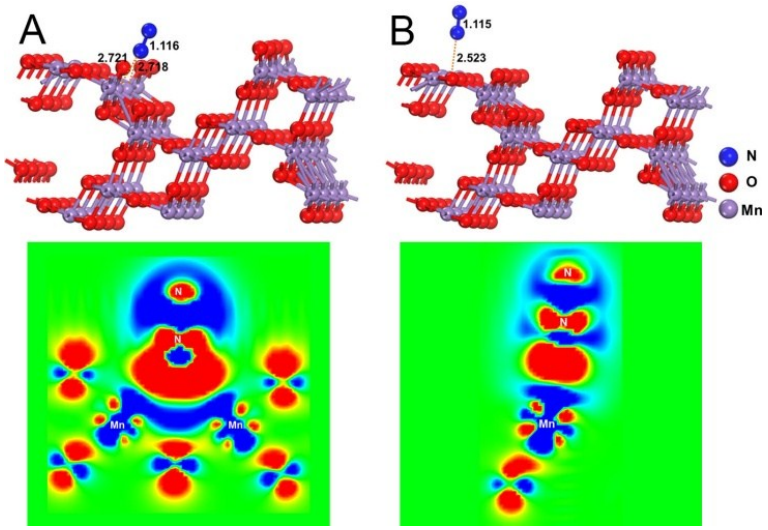

Fig. S22. Optimized structures and charge density difference of the N_2 adsorption on the MnO_2 (310) surfaces with (A) and without (B) V_O. Selected bond lengths (Å) are also given. Red and blue isosurfaces (0.001 a.u.) represent charge accumulation and depletion, respectively.

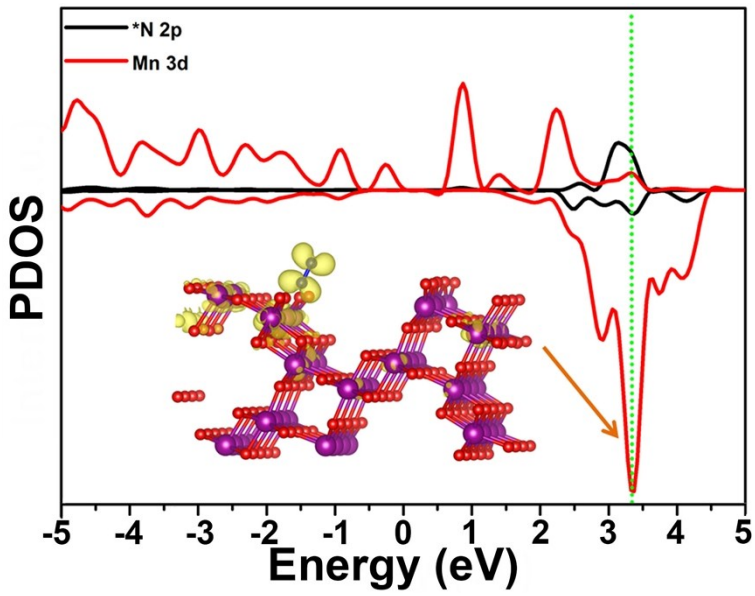

Fig. S23. PDOS profiles of N_2 adsorption on the MnO_2 (310) surface with one oxygen vacancy. In the end-on adsorption configuration, two Mn_{6c} atoms near the oxygen vacancy interact with N_2. The overlap between 3d of the two Mn_{6c} atoms and 2p of the adsorbed *N atom confirms the interaction between N_2 and MnO_2 surface (Charge density is inserted).

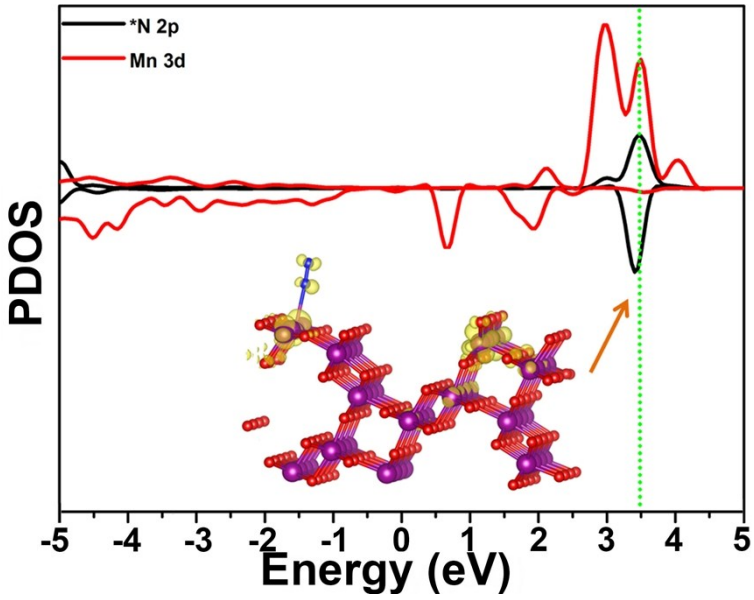

Fig. S24. PDOS profiles of N_2 adsorption on the pristine MnO_2 (310) surface. The exposed Mn_{5c} atom interacts with N_2. The overlap between 3d of the Mn_{5c} atom and 2p of the adsorbed *N atom confirms the interaction between N_2 and MnO_2 surface. (Charge density is inserted).

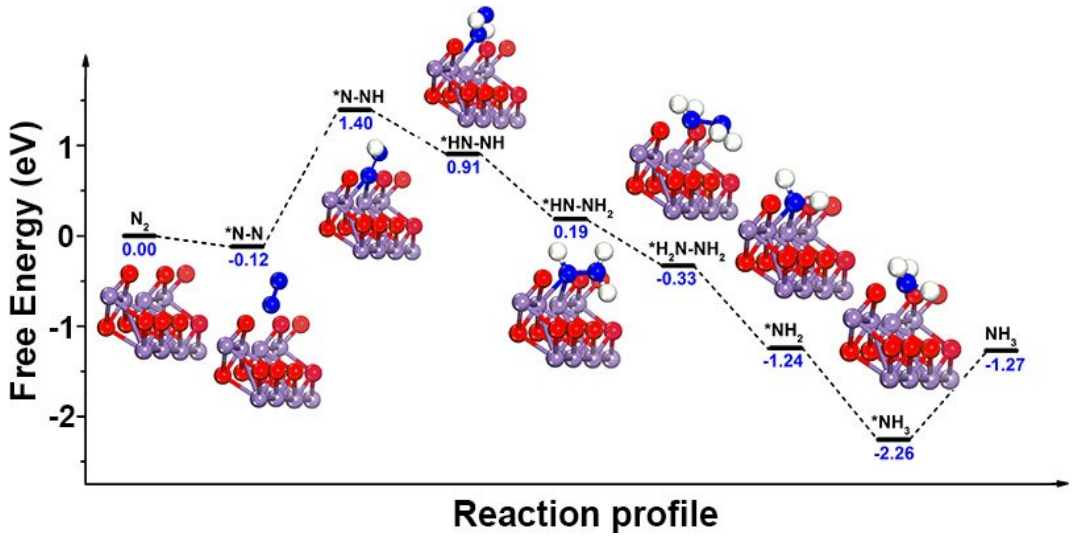

Fig. S25. DFT computed energy profile for the electrocatalytic NRR on the MnO_2 (310) surface with an oxygen vacancy.

One computed favorable energy profile for the NRR on the MnO_2 (310) surface with an oxygen vacancy is shown in Fig. S18. The N_2 adsorption energy is predicted to be 0.54 eV (free energy: 0.12 eV). After N_2 adsorption, six consecutive proton and electron transfer processes are involved along the alternative reaction pathway. Firstly, a hydrogen attacks the distal *N atom and forms the *N-NH species. Then, a second hydrogen attaches to the proximal N and generates the *HN-NH species. The following hydrogenation reactions alternately occur between these two N atoms resulting in two NH_3 molecules. The free energy changes along this reaction pathway are totally downhill except the reaction step from *N-N to *N-NH, which has a free energy barrier of 1.52 eV. It will be reduced to 1.02 eV with an external potential of -0.5 V vs. RHE.

Table S1. Comparison of the NRR performances for MnO_x NA/TM with reported NRR electrocatalysts under ambient conditions.

Catalyst	Electrolyte	NH_3 yield	FE (%)	Ref.
MnO_x NA/TM	**0.1 M Na_2SO_4**	**1.63×10^{-10} mol cm^{-2} s^{-1}**	**11.40**	**This work**
Fe_2O_3-CNT	diluted $KHCO_3$	3.59×10^{-12} mol cm^{-2} s^{-1}	0.15	1
SnO_2	0.1 M Na_2SO_4	1.47×10^{-10} mol cm^{-2} s^{-1}	2.17	11
MoS_2/CC	0.1 M Na_2SO_4	8.08×10^{-11} mol cm^{-2} s^{-1}	1.17	12
Fe_3O_4/Ti	0.1 M Na_2SO_4	5.6×10^{-11} mol cm^{-2} s^{-1}	2.6	13
TiO_2	0.1 M Na_2SO_4	9.16×10^{-11} mol cm^{-2} s^{-1}	2.5	14
TiO_2-rGO	0.1 M Na_2SO_4	15.13 μg h^{-1} $mg^{-1}_{cat.}$	3.3	15
defect-rich MoS_2 nanoflower	0.1 M Na_2SO_4	29.28 μg h^{-1} $mg^{-1}_{cat.}$	8.34	16
Hollow Cr_2O_3 microspheres	0.1 M Na_2SO_4	25.3 μg h^{-1} $mg^{-1}_{cat.}$	6.78	17
AuHNCs	0.5 M $LiClO_4$	6.37×10^{-11} mol cm^{-2} s^{-1}	30.2	18
N-doped C nanospikes	0.25 M $LiClO_4$	1.59×10^{-9} mol cm^{-2} s^{-1}	11.56	19
β-FeOOH nanorod	0.5 M Li_2SO_4	23.32 μg h^{-1} $mg^{-1}_{cat.}$	6.7	20
Pd/C	0.1 M PBS	4.5 μg h^{-1} $mg^{-1}_{cat.}$	8.2	21
Fe/Fe_3O_4	0.1 M PBS	3.06×10^{-12} mol cm^{-2} s^{-1}	8.29	22
Mo nanofilm	0.01 M H_2SO_4	3.09×10^{-11} mol cm^{-2} s^{-1}	0.72	23
BG	0.05 M H_2SO_4	1.6×10^{-10} mol cm^{-2} s^{-1}	10.8	24
$Ti_3C_2T_x$ nanosheet	0.1 M HCl	20.4 μg h^{-1} $mg_{cat.}^{-1}$	9.3	25
NPC	0.05 M H_2SO_4	23.80 μg h^{-1} $mg^{-1}_{cat.}$	1.42	26
TA-reduced Au/TiO_2	0.1 M HCl	21.40 μg h^{-1} $mg^{-1}_{cat.}$	8.11	27
$Bi_4V_2O_{11}/CeO_2$	0.1 M HCl	23.21 μg h^{-1} $mg^{-1}_{cat.}$	10.16	28
MoO_3	0.1 M HCl	29.43 μg h^{-1} $mg^{-1}_{cat.}$	1.9	29
Mo_2N	0.1 M HCl	78.4 μg h^{-1} $mg^{-1}_{cat.}$	4.5	30
MoN NA/CC	0.1 M HCl	3.01×10^{-10} mol cm^{-2} s^{-1}	1.15	31
NCM-Au NPs	0.1 M HCl	5.9×10^{-10} mol cm^{-2} s^{-1}	22	32
Nb_2O_5 nanofiber	0.1 M HCl	43.6 μg h^{-1} $mg^{-1}_{cat.}$	9.26	33
PCN	0.1 M HCl	8.09 μg h^{-1} $mg^{-1}_{cat.}$	11.59	34
B_4C	0.1 M HCl	26.57 μg h^{-1} $mg^{-1}_{cat.}$	15.95	35
Ag nanosheet	0.1 M HCl	4.62×10^{-11} mol cm^{-2} s^{-1}	4.8	36
ZIF-derived carbon	0.1 M KOH	9.44×10^{-10} mol cm^{-2} s^{-1}	10.20	37

References

1 S. Chen, S. Perathoner, C. Ampelli, C. Mebrahtu, D. Su and G. Centi, *Angew. Chem., Int. Ed.*, 2017, **56**, 2699–2703.

2 G. W. Watt and J. D. Chrisp, *Anal. Chem*., 1952, **24**, 2006–2008.

3 G. Kresse and J. Furthmüller, *Comput. Mater. Sci.*, 1996, **6**, 15–50.

4 G. Kresse and J. Furthmüller, *Phys. Rev. B*, 1996, **54**, 11169–11186.

5 Z. Fan, Z. Wang, J.-W. Shi, C. Gao, G. Gao, B. Wang, Y. Wang, X. Chen , C. He and C. Niu, *J. Catal.* 2019, **370**, 30–37.

6 J. P. Perdew, K. Burke and M. Ernzerhof, *Phys. Rev. Lett.*, 1996, **77**, 3865–3868.

7 G. Kresse and D. Joubert, *Phys. Rev. B*, 1999, **59***,* 1758–1775.

8 P. E. Blöchl, *Phys. Rev. B*, 1994, **50**, 17953–17979.

9 C. R. Podloucky, J. Paier, M. Marsman and G. Kresse, *Phys. Rev. B*, 2007, **75**, 195128.

10 G. Trimarchi and N. Binggeli, *Phys. Rev. B*, 2005, **71**, 035101.

11 L. Zhang, X. Ren, Y. Luo, X. Shi, A. M. Asiri, T. Li and X. Sun, *Chem. Commun.*, 2018, **54**, 12966–12969.

12 L. Zhang, X. Ji, X. Ren, Y. Ma, X. Shi, Z. Tian, A. M. Asiri, L. Chen, B. Tang and X. Sun, *Adv. Mater.*, 2018, **30**, 1800191.

13 Q. Liu, X. Zhang, B. Zhang, Y. Luo, G. Cui, F. Xie and X. Sun, *Nanoscale*, 2018, **10**, 14386–14389.

14 R. Zhang, X. Ren, X. Shi, F. Xie, B. Zheng, X. Guo and X. Sun, *ACS Appl. Mater. Interfaces*, 2018, **10**, 28251–28255.

15 X. Zhang, Q. Liu, X. Shi, A. M. Asiri, Y. Luo, X. Sun and T. Li, *J. Mater. Chem. A*, 2018, **6**, 17303–17306.

16 X. Li, T. Li, Y. Ma, Q. Wei, W. Qiu, H. Guo, X. Shi, P. Zhang, A. M. Asiri, L. Chen, B. Tang and X. Sun, *Adv. Energy Mater.*, 2018, **8**,1801357.

17 Y. Zhang, W. Qiu, Y. Ma, Y. Luo, Z. Tian, G. Cui, F. Xie, L. Chen, T. Li and X. Sun, *ACS Catal.*, 2018, **8**, 8540–8544.

18 M. Nazemi, S. R. Panikkanval and M. A. El-Sayed, *Nano Energy*, 2018, **49**, 316–323.

19 Y. Song, D. Johnson, R. Peng, D. K. Hensley, P. V. Bonnesen, L. Liang, J. Huang, F. Yang, F. Zhang, R. Qiao, A. P. Baddorf, T. J. Tschaplinski, N. L. Engle, M. C. Hatzell, Z. Wu, D. A. Cullen, H. M. Meyer III, B. G. Sumpter and A. J. Rondinone, *Sci. Adv.*, 2018, **4**, e1700336.

20 X. Zhu, Z. Liu, Q. Liu, Y. Luo, X. Shi, A. M. Asiri, Y. Wu and X. Sun, *Chem. Commun.*, 2018, **54**, 11332–11335.

21 J. Wang, Y. Liang, L. Hu, G. Chen, H. Xin and X. Feng, *Nat. Commun.*, 2018, **9**, 1795.

22 L. Hu, A. Khaniya, J. Wang, G. Chen, W. E. Kaden and X. Feng, *ACS Catal.*, 2018, **8**, 9312–9319.

23 D. Yang, T. Chen and Z. Wang, *J. Mater. Chem. A*, 2017, **5**, 18967–18971.

24 X. Yu, P. Han, Z. Wei, L. Huang, Z. Gu, S. Peng, J. Ma and G. Zheng, *Joule*, 2018, **2**, 1610–1622.

25 J. Zhao, L. Zhang, X.-Y. Xie, X. Li, Y. Ma, Q. Liu, W.-H. Fang, X. Shi, G. Cui and X. Sun, *J. Mater. Chem. A*, 2018, **6**, 24031–24035.

26 Y. Liu, Y. Su, X. Quan, X. Fan, S. Chen, H. Yu, H. Zhao, Y. Zhang and J. Zhao, *ACS Catal.*, 2018, **8**, 1186−1191.

27 M. Shi, D. Bao, B. Wulan, Y. Li, Y. Zhang, J. Yan and Q. Jiang, *Adv. Mater.*, 2017, **29**, 1606550.

28 C. Lv, C. Yan, G. Chen, Y. Ding, J. Sun, Y. Zhou and G. Yu, *Angew. Chem., Int. Ed.,* 2018, **57,** 6073–6076.

29 J. Han, X. Ji, X. Ren, G. Cui, L. Li, F. Xie, H. Wang, B. Li and X. Sun, *J. Mater. Chem. A*, 2018, **6**, 12974–12977.

30 X. Ren, G. Cui, L. Chen, F. Xie, Q. Wei, Z. Tian and X. Sun, *Chem. Commun.*, 2018, **54**, 8474–8477.

31 L. Zhang, X. Ji, X. Ren, Y. Luo, X. Shi, A. M. Asiri, B. Zheng and X. Sun,

ACS Sustainable Chem. Eng., 2018, **6**, 9550–9554.

32 H. Wang, L. Wang, Q. Wang, S. Ye, W. Sun, Y. Shao, Z. Jiang, Q. Qiao, Y. Zhu, P. Song, D. Li, L. He, X. Zhang, J. Yuan, T. Wu and G. A.O. zin, *Angew. Chem., Int. Ed.*, 2018, **57**, 12360–12364.

33 J. Han, Z. Liu, Y. Ma, G. Cui, F. Xie, F. Wang, Y. Wu, S. Gao, Y. Xu and X. Sun, *Nano Energy*, 2018, **52**, 264–270.

34 C. Lv, Y. Qian, C. Yan, Y. Ding, Y. Liu, G. Chen and G. Yu, *Angew. Chem., Int. Ed.*, 2018, **57**, 10246–10250.

35 W. Qiu, X. Xie, J. Qiu, W. Fang, R. Liang, X. Ren, X. Ji, G. Cui, A. M. Asiri, G. Cui, B. Tang and X. Sun, *Nat. Commun.*, 2018, **9**, 3485.

36 H. Huang, L. Xia, X. Shi, A. M. Asiri and X. Sun, *Chem. Commun.*, 2018, **54**, 11427–11430.

37 S. Mukherjee, D. A. Cullen, S. Karakalos, K. Liu, H. Zhang, S. Zhao, H. Xu, K. L. More, G. Wang and G. Wu, *Nano Energy*, 2018, **48**, 217–226.